J. Biochem., 77, 147–162 (1975)

The Crystal Structure of Bonito (Katsuo) Ferrocytochrome *c* at 2.3 A Resolution

II. Structure and Function

Nobuo TANAKA, Takashi YAMANE,[1] Tomitake TSUKIHARA,[2] Tamaichi ASHIDA,[3] and Masao KAKUDO

Institute for Protein Research, Osaka University, Suita, Osaka 565

Received for publication, June 17, 1974

The structure analysis of bonito heart ferrocytochrome *c* was carried out at 2.3 A resolution by X-ray diffraction, and a Kendrew-type skeletal model was built up. This molecule has an overall egg shape, 35 A in height, 30 A in width and 23 A in thickness; the 5th ligand of the heme iron atom is the N^{ϵ} atom of the His-18 imidazole ring and the 6th is the Met-80 sulfur atom. Distinct α-helix regions are found between the N-terminus and residue 11, between 60 and 69, and between 90 and the C-terminus. The most distinct difference between the conformation of the present molecule and that of the horse oxidized molecule is the location of the Phe-82 phenyl ring. In the present reduced molecule, the phenyl ring is in closer contact with the iron atom and gives influences on the character of the iron atom. Inside the molecule, at the lower part of the heme pocket, there is an extended hydrogen bond network including the propionic acid residues of the heme group. Both Phe-82 and the hydrogen bond network may play a key role in the function of this molecule.

All aerobic organisms contain a group of intercellular hemoprotein enzymes, the cytochromes, which are involved in the major pathway of biological oxidation. This system is present chiefly in the mitochondria of the cell. One member of the group, cytochrome *c*, interacts with cytochrome reductase and oxidase, and plays a role in transferring one electron from the former to the latter. The cytochrome *c* undergoes respetitive oxidation and reduction of the iron atom as its integral function. Bonito cytochrome *c* consists of a single peptide chain of 103 amino acid residues and one heme *c* which is covalently linked to the peptide chain by two thioether linkages at Cys-14 and -17. The amino acid sequence determined by Nakayama *et al.* (*1*) is shown in Fig. 1.

Crystal structure analysis of bonito ferrocytochrome *c* has been carried out by the authors. The structure at 4.0 A resolution

[1] Present address: Faculty of Engineering, Nagoya University, Chikusa-ku, Nagoya.

[2] Present address: Faculty of Engineering, Tottori University, Tottori.

[3] Present address: Faculty of Engineering, Nagoya University, Chikusa-ku, Nagoya.

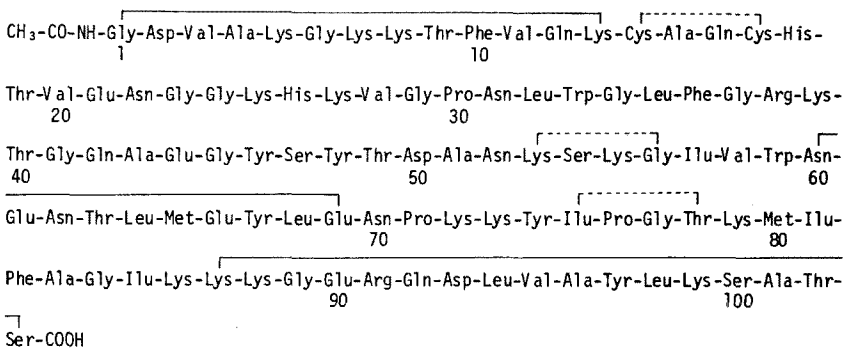

Fig. 1. The amino acid sequence of bonito cytochrome *c* (*1*).

and the preliminary results at 2.3 A were reported in previous papers (*2*, *3*). The cytochrome *c* was oxidized into ferric form in the crystalline state, retaining isomorphism with the native crystal. An X-ray study of this oxidation process was also reported previously (*4*). In the present paper, the detailed structural characteristics of bonito ferrocytochrome *c* are reported and the relation between the structures and their function is briefly discussed.

Dickerson, Takano, and others have reported the structure of horse ferricytochrome *c* at 2.8 A (*5*) and of tuna ferrocytochrome *c* at 2.45 A (*6*), and proposed a mechanism for electron transfer based on the difference in structure between the ferric and ferrous forms.

The overall features of the present molecule are very similar to those of ferricytochrome *c* presented by Dickerson. Although no dramatic differences between the ferric and ferrous forms of this protein have been found, some specific structures of this protein will be discussed in comparison with those of the horse ferric and tuna ferrous forms.

EXPERIMENTAL

The preparation and crystallization of cytochrome *c* was previously reported at 4.0 A resolution (*2*). The crystallographic data are listed in Table I. In the analysis at 4.0 A, two heavy atom-replaced crystals containing $K_3UO_2F_5$ (U derivative) and K_2PtCl_4 (Pt derivative) were utilized for phase angle determination. The Pt derivative was found to be rather poor in both crystallinity and isomorphism, so it was not used in the present analysis.

TABLE I. Crystallographic data.

Space group	$P2_12_12_1$ (orthorhombic)
Cell dimensions	a=57.68 A[a]
	b=84.58
	c=37.83
Molecular weight	12,024
Observed density	ρ_0=1.38 g/cm^3
The number of molecules in the unit cell	Z=8
The number of molecules per asymmetric unit	2
Water content	35 w/w %

[a] This crystal has a pseudo identity period along the a axis. The reduced cell has a=28.84 A and a space group of $P22_12_1$.

For the analysis at 2.3 A resolution, further trials to find new heavy atom reagents were carried out. The X-ray intensity data of some derivatives using $(CH_3)_2SnCl_2$, K_3IrCl_6, CdI_2, $UO_2(CH_3COO)_2$, $K_2Pt(SCN)_6$, and K_2HgI_4 were collected within 4.0 A resolution in order to check the suitability of the diffraction data. Soaking with $UO_2(CH_3COO)_2$ broadens the profile of the diffraction spot, so that this reagent could not be used for analysis at the higher resolution. The occupancies of CdI_2 and $K_2Pt(SCN)_6$ at each definite site are very low. When the concentration of CdI_2 was increased in the soaking solution, the difference Fourier map was confused by trivial electron density

humps, which showed the displacement of the peptide chain or many heavy atom sites with small degrees of occupancy. In the case of $K_2Pt(SCN)_6$, when the crystal was soaked in a high concentration of the reagent, the diffraction spots disappeared, because of denaturation of the protein. K_2HgI_4 seemed to be suitable at first, but at the stage of refinement, the parameters of the heavy atom could not be refined well. Two new compounds, $(CH_3)_2SnCl_2$ (Sn derivative) and K_3IrCl_6 (Ir derivative), were found suitable for the structure determination. The concentration of the heavy atom reagents in the soaking solutions, and the soaking times are;

U derivative	45	mM	3 days[4]
Sn derivative	2.3	mM	4 days
Ir derivative	19	mM	5 days

Throughout the experiments, the oxidation of protein was carefully avoided. Thus, a small amount of ascorbic acid was contained in the soaking solution for the Sn and Ir derivatives. For the U derivative, the crystal was reduced for half a day with ascorbic acid added to the soaking solution after the end of soaking, because the heavy atom reagent reacts with ascorbic acid. Air dissolved in the soaking solution was replaced with nitrogen gas. In collecting the intensity data, the crystal was sealed in a capillary filled with nitrogen gas. The percentage reduction of the crystal was improved by these procedures. After the measurement of intensities, the percentages of reduction estimated from the visible light spectrum at 550 nm were above 80% in all cases.

Intensity data for about 8,000 reflections for each of the native material and three derivatives were measured on a Rigaku Denki computer-controlled four-circle diffractometer (AFC-III), using Cu-K_α radiation filtered with nickel foil. Reflections were continuously scanned along the ω-axis. For the native crystal, three sets of intensity data were collected in order to estimate the experimental error.

[4] This condition is same as that in the 4.0 A analysis.

STRUCTURE DETERMINATION

Preliminary data processing, that is the Lp correction, Furnas-type absorption correction, Wilson's plot and so on, were carried out as described for the 4.0 A analysis (*2*). The difference Fourier map was prepared in order to find the heavy atom binding sites, using the best phase angles at 4.0 A. The positional parameters, temperature factors and occupancies of the heavy atoms were refined by least-squares calculation. About 1,500 reflections within the 2.3 A range which were comparatively strong for the native crystal and all the derivatives, were used for this calculation.

Some statistical details of the phase angle determination are shown in Fig. 2 and the parameters of the heavy atoms are listed in Table II. Among the three derivatives, the U derivative was the best one, while the Ir derivative had rather small occupancies, and was not so effective for phase angle determination. The Sn derivative worked well for reflections of rather high orders and broke the pseudo-translational symmetry along the a axis, because the occupancy of Sn-3 is negligibly smaller than that of Sn-2, the two sites being related by the pseudo symmetry. On the other hand, the U and Ir derivatives retained this pseudo symmetry.

After many cycles of refinement of these

TABLE II. Heavy atom parameters.

	x/*a*	y/*b*	z/*c*	Occupancy[a]
$K_3UO_2F_5$				
U-1	0.0897	0.1317	0.0506	42.0
U-2	0.5863	0.1412	0.0807	69.8
$(CH_3)_2SnCl_2$				
Sn-1	0.8950	0.2473	0.0513	12.0
Sn-2	0.8182	0.4466	0.1964	63.0
Sn-3	0.3537	0.4682	0.1738	6.2
K_3IrCl_6				
Ir-1	0.4250	0.2676	0.2108	10.3
Ir-2	0.9317	0.2596	0.2027	15.0

[a] In units of eA^{-3}.

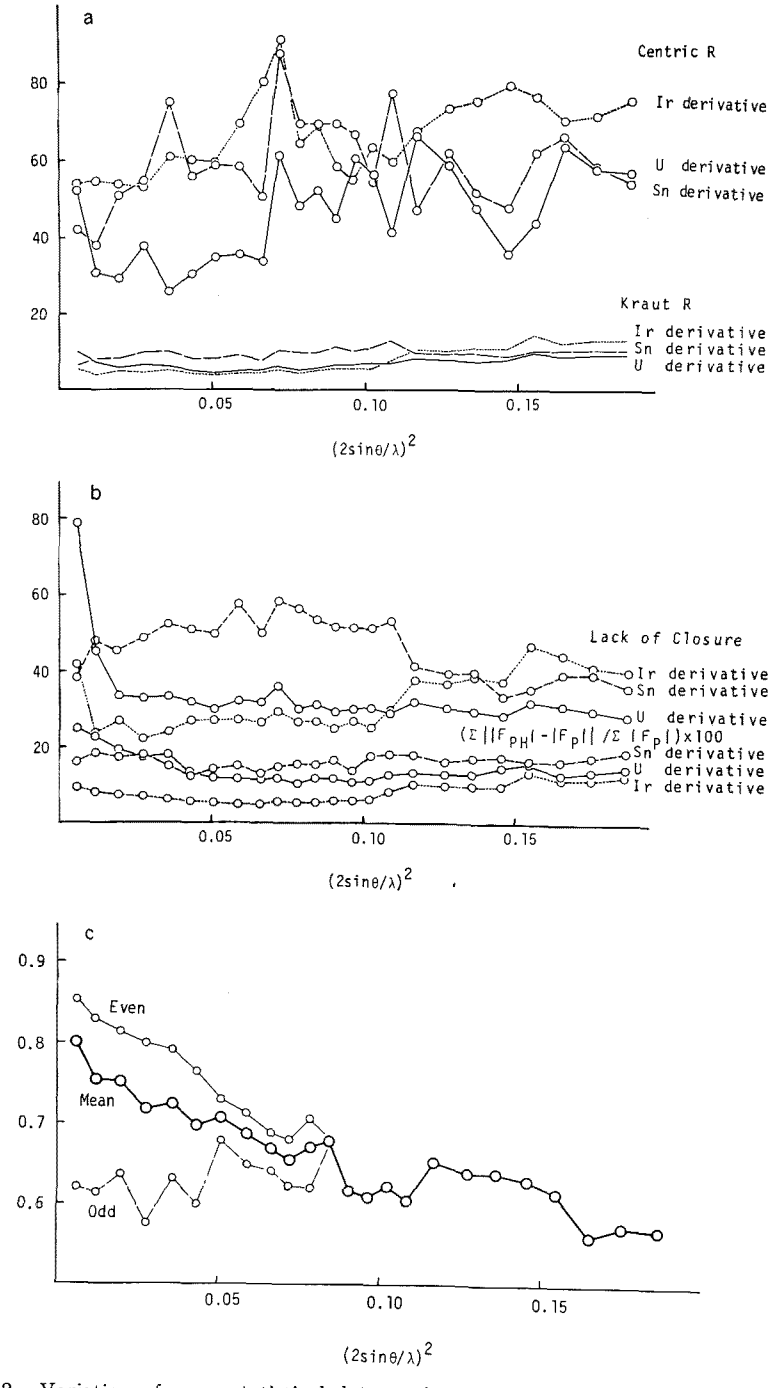

Fig. 2. Variation of some statistical data against ($\sin\theta/\lambda$). (a) Centric R and Kraut R of the three derivatives. (b) The r.m.s. value of lack of closure calculated with the final phase angles. $\sum||F_{PH}|-|F_P||/\sum|F_P|$ is the mean change in protein structure factors produced by the heavy atom reagents. (c) Figure of merit. The subscripts, even and odd, show the averaged figure of merit of the reflections with h even and odd, respectively. The 'mean' represents the figure of merit calculated with all significant reflections. From this figure, the present analysis above 4.0 A resolution does not suffer from the pseudo symmetry seen in 4.0 A analysis.

TABLE III. Amino acid residues nearest to the heavy atom sites.

$UO_2F_5^{3-}$	Glu-90
$UO_2(CH_3COO)_2$	Glu-90
$(CH_3)_2SnCl_2$ (main)	Cys-17
$(CH_3)_2SnCl_2$ (minor)	Glu-61, Lys-99
$IrCl_6^{3-}$	Asn-60, Glu-61
$PtCl_4^{2-}$	Met-65
HgI_4^{2-} (main)	Cys-17

heavy atom parameters, the best phase angles and the best electron density distribution were calculated. About 5,200 reflections which were significantly above the background intensity were used for this synthesis. The phase probability was estimated using the formula

$$P(\alpha)=N\cdot\exp[-\sum_i\{\varepsilon_i^2(\alpha)/2E_i^2\}]$$

which was intermediate between the formula proposed by Blow and Crick (*7*) and that of Cullis *et al.* (*8*). In the present formula, E_i is the standard deviation of the structure factors of the *i*-th derivative, E_i for the native crystal being estimated from the r.m.s. differences among three sets of data. The mean figure of merit averaged over all reflections was 0.65.

Heavy Atom Binding Sites—The binding sites of the heavy atom groups are listed in Table III. The binding site of $UO_2(CH_3COO)_2$ is the same as that of $K_3UO_2F_5$. The main binding site of the organo-tin molecule was found to be close to the thioether bridge of Cys-17 joining the heme group, Cys-17 being on the surface of the molecule. This site was almost the same as that of K_2HgI_4. The parameters of the site in the tin-replaced crystal could be reasonably well refined, but on the other hand, the Hg reagent appreciably affected the isomorphism and could not be used for phase angle determination.

STRUCTURE

The electron density map was carefully scrutinized in a Richard box, and a Kendrew-type skeletal model was built up. A schematic drawing of the model is shown in Fig. 3 and

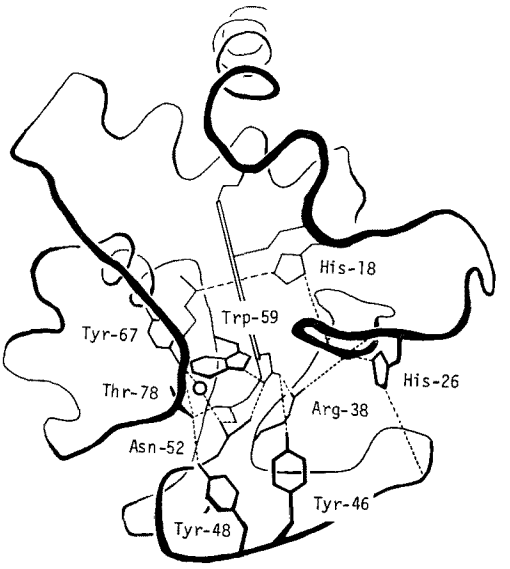

Fig. 3. Schematic drawing of the main chain folding viewed from the front. The dotted lines show intramolecular hydrogen bonds. The open circle represents the water molecule fixed with hydrogen bonds.

stereoscopic drawings are also shown in Figs. 4, 5, and 6. The most prominent feature in the electron density map is the planar heme group, with two dense peaks of the sulfur atoms of Cys-14 and -17 located close to the corner of the heme plane. The fitting between the electron density map and the heme plane is shown in Fig. 7. Only one edge of the heme is exposed to the outer medium, at the Cys-17 thioether linkage.

The bonito ferrocytochrome *c* has an overall egg shape. It is 35 A in height, 30 A in width, and 23 A in thickness. There is a large crevice at the upper right part of the molecule. The 5th ligand of the heme is the N^{ε} atom of the His-18 imidazole ring and the 6th is the Met-80 sulfur atom, which are consistent with horse ferricytochrome *c* (*5*) and tuna ferrocytochrome *c* (*6*). There are several helical segments. Distinct α-helix regions are found between the N-terminus and residue 11 (H-1), between 60 and 69 (H-2), and between 90 and the C-terminus (H-3). The H-1 helix is about 2.5 turns, and runs from the back to the front at the top of the molecule. The H-2

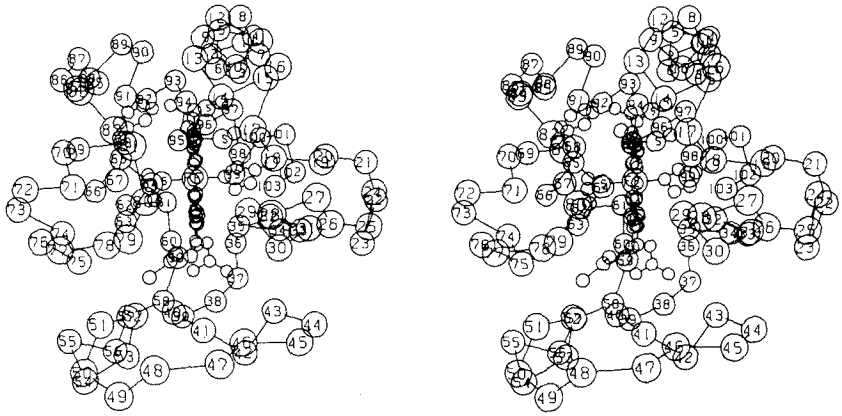

Fig. 4. Stereoscopic drawing of α-carbon and heme, viewed from the front.

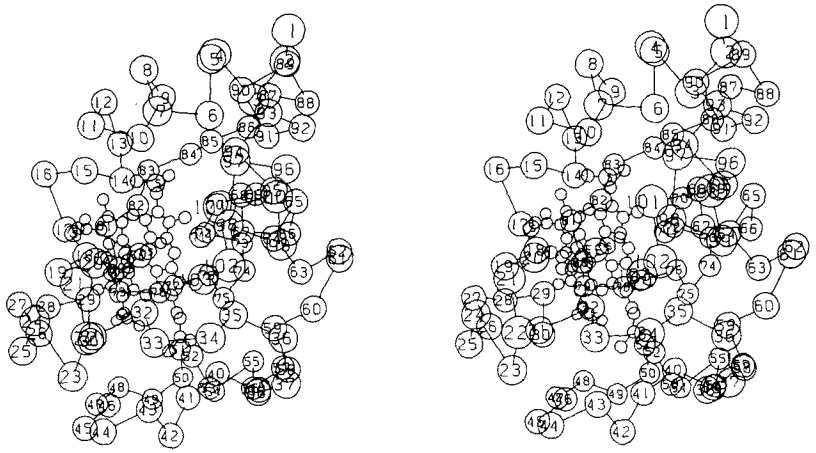

Fig. 5. Stereoscopic drawing, right view.

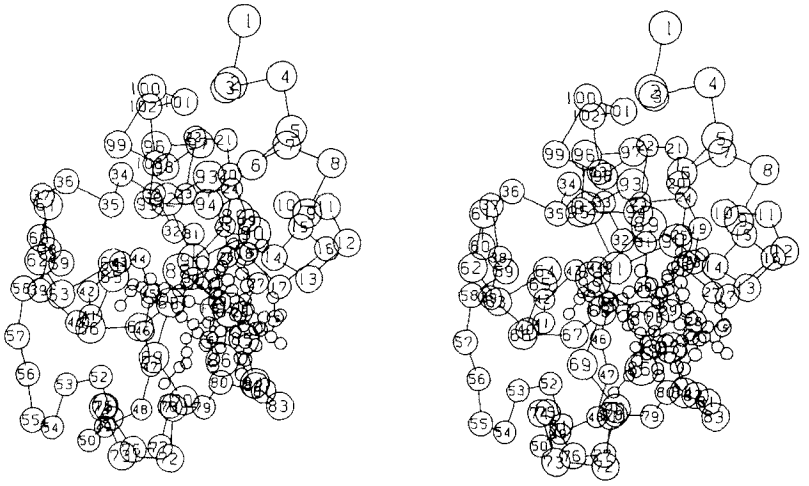

Fig. 6. Stereoscopic drawing, top view from the left rear side.

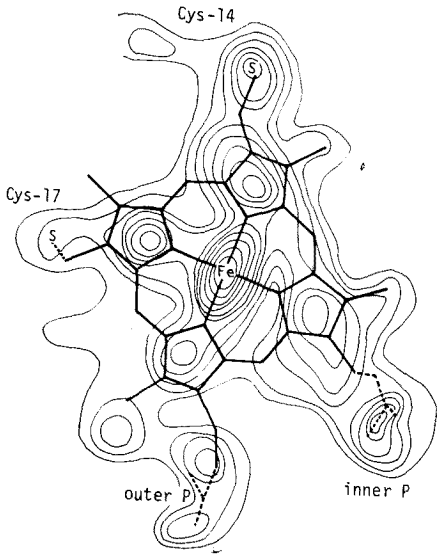

Fig. 7. A composite drawing of the electron density distribution on the heme plane. An idealized heme skeleton is superimposed at the same scale. Contours are at zero and equal intervals of 0.2 e/A^3 above the average density.

helix, about 2 turns, is located at the back. The H-3 helix is as long as 4 turns, and is at the upper rear part of the molecule. These helices show perfect hydrogen bond networks between the carbonyl and amido groups.

Other helical segments are found from residues 14 to 17, and from 49 to 55. The former takes a 3_{10} conformation (type 1) (*9*) with the hydrogen bond between the carbonyl of Cys-14 and the amido of Gln-16. The latter contains the hydrogen bond between residues 49 and 53, and between 53 and 55. The chain folding from 53 to 55 corresponds to the 3_{10} conformation, but it is coiled loosely from 49 to 53. Dickerson found several 3_{10} conformations in horse ferricytochrome *c* (*5*). The 3_{10} conformations found in horse and bonito are listed in Table IV. In the case of bonito ferrocytochrome *c*, that from residues 61 to 70 is an α-helix (H-2), and those from 21 to 24 and between 35 and 38 are not found, though that from 75 to 78 is consistent with the results for the ferric form.

The aromatic ring can be assigned unambiguously in the electron density map. The Phe-82 phenyl ring stands roughly parallel to the heme plane and, in comparison with the structure of horse ferric form, moves towards the heme plane from the exterior with a slight refolding of the main chain from 80 to 82, closing the left channel found in horse ferric form. The positions of Tyr-67, Trp-59, and Tyr-74 are interesting in relation to the electron transfer mechanism discussed later. The agreement between the skeletal model and the electron density map of this part is shown in Fig. 8. It was reported for the ferric form (*5*) that the Tyr-67 phenyl ring is parallel to the heme plane and the rings of Trp-59 and Tyr-74 are also folded over each other. In the present results, the overlaps between the ring of Trp-59 and Tyr-74, and between Tyr-67 and

TABLE IV. 3_{10} Bends in horse and bonito cytochrome *c*.

Residue		Horse		Bonito	
C=O	NH	Type	Amino acid sequence	Type	Amino acid sequence
21	24	II	Gln-Lys-Gly-Gly		
35	38	II	Leu-Phe-Gly-Arg		
61	64	I	Glu-Glu-Thr-Leu	[a]	Glu-Asn-Thr-Leu
66	69	I	Glu-Tyr-Leu-Glu	[a]	Glu-Tyr-Leu-Glu
67	70	I	Tyr-Leu-Glu-Asn	[a]	Tyr-Leu-Glu-Asn
75	78	II	Ilu-Pro-Gly-Thr	II	Ilu-Pro-Gly-Thr
53	56			I	Lys-Ser-Lys-Gly
14	17			I	Cys-Ala-Glu-Cys

[a] In the H-2 helix in bonito.

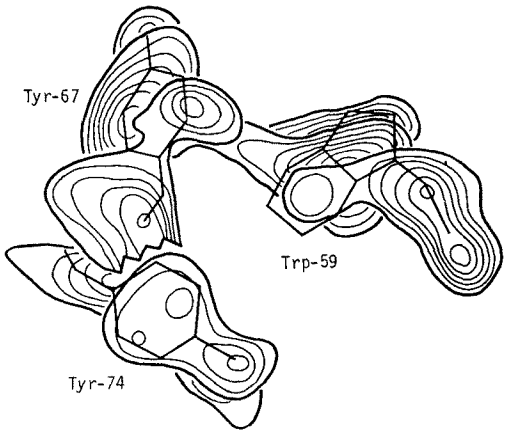

Fig. 8. Comparison of the electron density distribution with the locations of the aromatic rings. The contours begin at 0.2 e/A^3 above the average density, with equal intervals of 0.1 e/A^3.

Trp-59 are not as appreciable, though Tyr-67 and Trp-59 may be recognized as nearly parallel. Tyr-67 is not parallel to the heme plane and is not folded over the heme plane in bonito (Fig. 9).

TABLE V. The dihedral angle between the best plane of heme, Trp-59, Tyr-67, and Tyr-74.

	Bonito	Tuna	Horse
Heme ····· Trp-59	67°	54°	65°
Heme ····· Tyr-67	87	67	25
Heme ····· Tyr-74	95	80	49
Trp-59 ····· Tyr-67	21	59	65
Trp-59 ····· Tyr-74	45	41	16
Tyr-67 ····· Tyr-74	39	54	53

The hydrophobic groups aggregate at the upper half of the molecule. Only Ala-43, Ala-51, Ilu-57, Val-58, and Ilu-75 are in the lower part of the molecule. All 6 valyl residues are towards the exterior. About a half of the glycyl and alanyl residues are exposed to the outer medium. The leucyl and isoleucyl residues are buried inside the molecule except for Ilu-81. The upper part of the heme pocket is mainly composed of hydrophobic residues such as Leu-32, Leu-35, Leu-64, Leu-68, Ilu-85, Leu-93, Leu-98, and Ala-101.

TABLE VI-a. Hydrogen bonds between carbonyl and amido groups in the main chain.

C=O	NH	Distance (A)	C=O	NH	Distance (A)
Gly-1	Lys-5	3.5[a]	Asn-62	Glu-66	2.6[b]
Asp-2	Gly-6	3.0[a]	Thr-63	Tyr-67	2.7[b]
Val-3	Lys-7	3.0[a]	Leu-64	Leu-68	2.4[b]
Ala-4	Lys-8	3.5[a]	Met-65	Glu-69	2.6[b]
Lys-5	Thr-9	2.9[a]			
Gly-6	Phe-10	2.5[a]	Lys-87	Arg-91	2.9[c]
Lys-7	Val-11	2.8[a]	Lys-88	Gln-92	2.6[c]
Lys-8	Gln-12	3.1[a]	Gly-89	Asp-93	2.7[c]
Thr-9	Lys-13	2.8[a]	Glu-90	Leu-94	2.6[c]
			Arg-91	Val-95	3.2[c]
Cys-14	Cys-17	2.9	Gln-92	Ala-96	3.0[c]
Arg-38	Trp-59	2.6	Asp-93	Tyr-97	2.8[c]
Thr-49	Ser-59	2.6	Leu-94	Leu-98	3.3[c]
Ilu-75	Thr-78	2.7	Val-95	Lys-99	3.3[c]
Lys-53	Gly-56	2.5	Ala-96	Ser-100	3.1[c]
			Tyr-97	Ala-101	2.8[c]
Asn-60	Leu-64	3.3[b]	Leu-98	Ser-103	2.7[c]
Glu-61	Met-65	3.2[b]			

[a] In the H-1 helix. [b] In the H-2 helix. [c] In the H-3 helix.

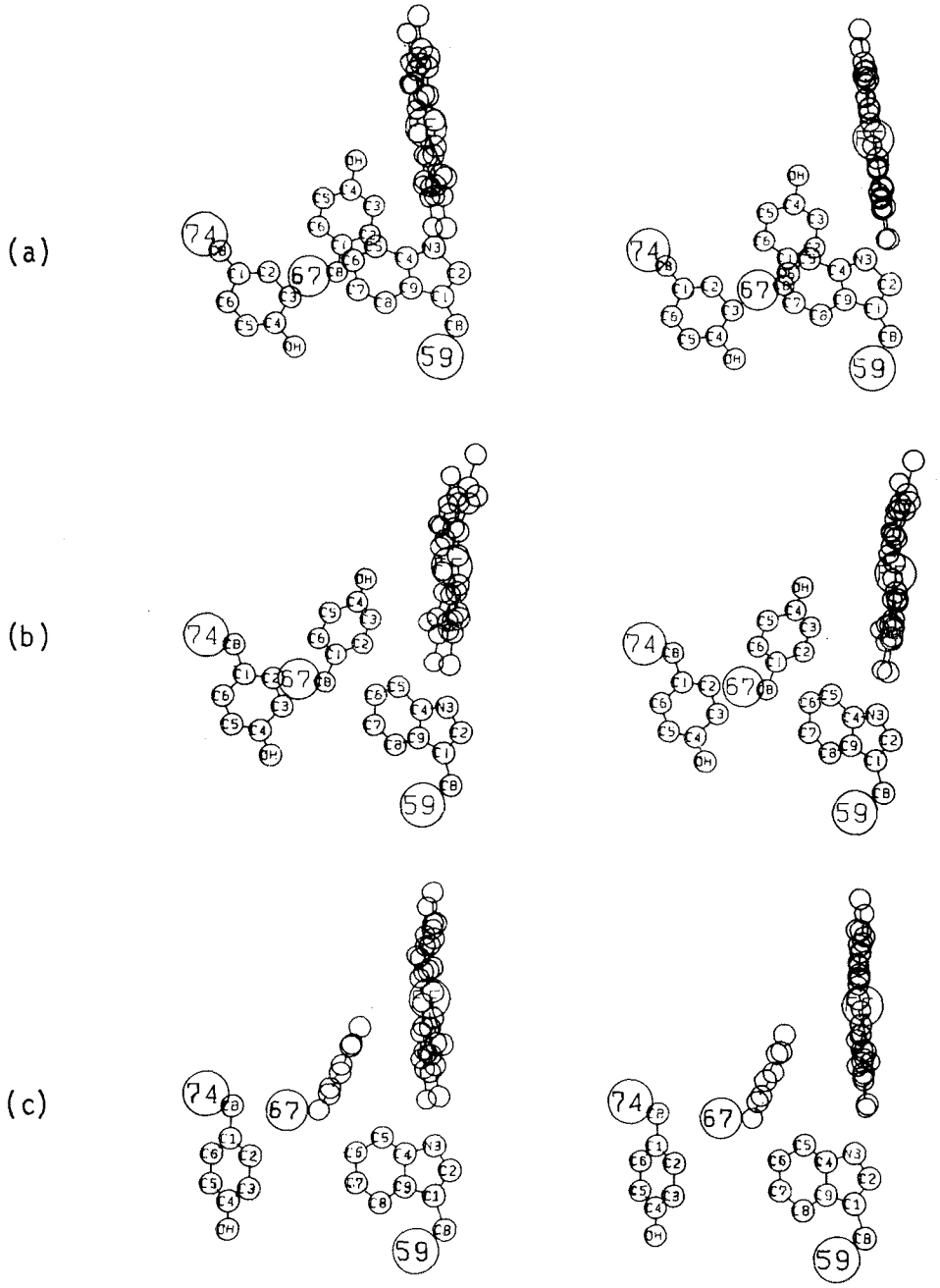

Fig. 9. Stereoscopic drawing of the relative locations of heme, Tyr-67, Trp-59, and Tyr-74. (a) Present bonito ferrous form. (b) Tuna ferrous form. (c) Horse ferric form.

TABLE VI-b. The intramolecular hydrogen bond pattern of the side groups. Inner P and outer P mean the inner and the outer propionic residues, respectively. (S) is a side group, (CO) is a carbonyl group, and (NH) is an amino group of each residue. The last column shows the distances in the present bonito ferrocytochrome *c*. The data for horse and tuna are from Dickerson's table (*5*).

	Horse	Tuna	Bonito	Distance
Tyr-46		outer P	inner P	2.8
-48	inner P	inner P	Thr-78 (S)	3.2
-67	Thr-78	Thr-78	Thr-78 (S)	3.2
			H_2O	2.5
-74			Thr-63 (S)	2.3
Thr-19	Lys-25	Lys-25	Lys-25 (CO)	2.8
-40	Lys-55	Lys-55	Asn-52 (S)	3.0
-49	outer P	outer P		
-63		Asn-60	Tyr-74 (S)	2.3
-78	Tyr-67	Tyr-67	Tyr-67	
			Tyr-48 (S)	2.6
			outer P	2.8
His-18	Pro-30	Pro-30	Pro-30 (CO)	3.5
-26	Pro-44	Gly-45	Glu-44 (CO)	2.8
			Asn-31 (NH)	2.6
Trp-33			Ala-43 (CO)	3.5
-59	inner P	inner P	inner P	3.1
Asn-31			Glu-21 (CO)	2.6
			Thr-19 (S)	2.7
-52	outer P	inner P	outer P	2.5
			inner P	2.9
			Thr-40 (S)	3.0
			H_2O	2.5
Gln-16			Val-11 (CO)	2.5
-42	Arg-38			
Arg-38	Gln-42		Gly-41 (CO)	3.0
			inner P	2.5

Bonito cytochrome *c* contains 16 lysyl residues, of which 9 residues protrude to the outer medium in the left rear corner of the molecule. The side chain of Lys-79 runs from left to right, covering the exposed lower front side of the heme. There is typical hydrophilic cluster on the surface at the top of the left rear, composed of Lys-5, Lys-8, Thr-9, Glu-12, Lys-13, Lys-86, Lys-87, Glu-90, Glu-92, and Asp-93. The rear of the molecule is crowded with Lys-55, Asn-60, Glu-61, Asn-62, Thr-63, Met-65, Glu-66, Glu-69, Asn-70, Lys-72, and Lys-73 (Fig. 5). These two clusters are in contact with each other. The right side and bottom of the molecule include several hydrophilic residues, but no clusters or groups of

hydrophilic residues, can be recognized.

Intramolecular hydrogen bonds are listed in Table VI-a and VI-b. Hydrogen bonds are held well in the three α-helix regions. The H-3 helix is deformed at the C-terminus, as shown by the hydrogen bond between Leu-98 and Ser-103. The hydrogen bond between Arg-38 and Trp-59 links two main chains which run antiparallel with each other at the back of the molecule (Fig. 5). Several hydrophilic side chains are oriented inward so as to form hydrogen bonds, for instance, the side group of Asn-31 makes a hydrogen bond with the carbonyl group of Glu-21 and the side group of Thr-19. The other polar residues inside the molecule are Arg-38, Thr-40, Tyr-46, Tyr-48, Asn-52, Trp-59, Tyr-67, Tyr-74, Thr-78, and two propionic residues. These residues constitute an extended hydrogen bond network at the lower part of the molecule, as shown in Fig. 10. Thr-78 seems to make three hydrogen bonds with Tyr-48, Tyr-67 and on outer propionic residue. Two propionic residues are combined with Asn-52. The inner propionic residue makes two more hydrogen bonds with Trp-59 and Arg-38. Arg-38 is fixed by three hydrogen bonds with an inner propionic residue, Asn-31 and Gly-41. A high electron density region found between the oxygen atom of the Tyr-67 ring and the carbonyl group of Asn-52 may be assigned to a water molecule. Thus, Tyr-67 links to Asn-52 *via* the water molecule. Another hydrogen bond chain is found in the front of the molecule, between the $N^{\delta'}$ of the His-18 imidazole ring··· the carbonyl of Pro-30; the amido of Asn-31··· the N^{ε} of the His-26 imidazole ring; and the $N^{\delta'}$ of the His-26 imidazole ring··· the carbonyl of Glu-44.

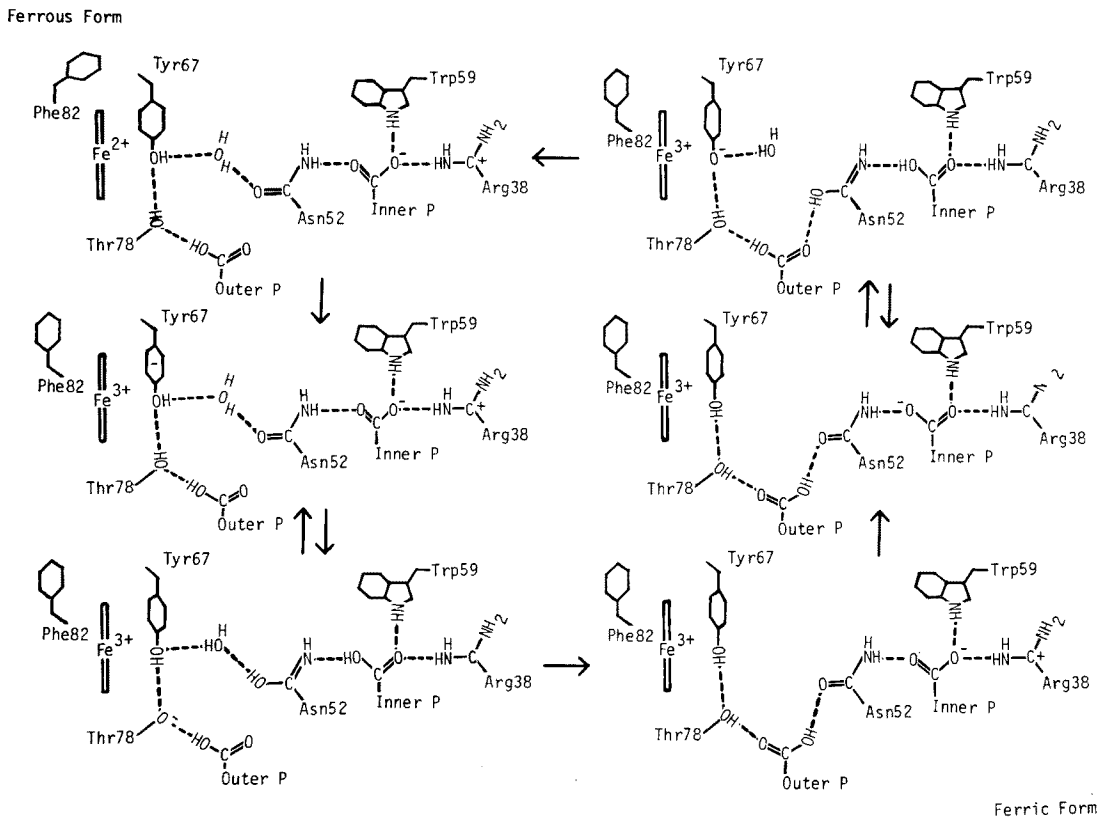

Fig. 10. Proposed scheme of electron transfer mechanism. The ferrous form (left top) is converted to the ferric form (right bottom) with rearrangement of the hydrogen bond pattern and movement of Phe-82. See the text for details.

DISCUSSION

It is of great interest to investigate the structural relations between the reduced and oxidized states. Only the Phe-82 phenyl ring takes a remarkably different position in the two states. This positional shift can be reasonably interpreted as due to the structural specificity of the main chain folding of this part, because the main chain between residues 81 and 86 has neither a hydrogen bond nor a close van der Waals contact with other parts of the molecule, so that this part may be flexible. From the 2.4 A analysis of tuna ferrocytochrome *c* (*6*), Takano *et al.* also reported that several minor changes occur between the ferric and ferrous forms. One of these changes is that the Trp-59 indole ring shifts upwards so as to come near the heme methyl at 3.0 A in the reduced state. In the present analysis, a bulky electron density hump is found at the indole ring of Trp-59, so that this ring may swing around the C_α-C_β bond. The position of the Tyr-74 ring in bonito and tuna is different from that in the horse ferric form (*4*). The ring protrudes towards the outer medium in the oxidized state, while it is buried in the molecule with a hydrogen bond to the side group of Thr-63 in the reduced state. Tyr-46 and -48 in bonito take different positions from those in horse and tuna, where each of these two residues takes almost the same position, despite the difference in degree of oxidation. In the present model Tyr-46 makes a hydrogen bond with inner propionic acid (inner P) and Tyr-48 also makes a hydrogen bond with Thr-78. In the horse ferric form and tuna ferrous form, Tyr-48 makes a hydrogen bond with inner P, and Tyr-46 in tuna, with outer propionic acid (outer P).

The 5th ligand side of the heme plane is in the heme crevice, and is not accessible from the front, the Cys-17 side, of the molecular surface. In the present protein, there is a large channel at the upper right of His-18, through which a small molecule or an ion may slip into the heme crevice from the outside of the molecule (Fig. 5). This channel is also open in the horse ferric form, though it is closed in the tuna ferrous form, mainly by Glu-21, Asn-22, and by the big indole ring of Trp-33. The Trp-33 indole ring goes downwards in bonito, but it goes upwards in tuna. The His-33 imidazole ring in horse goes downwards as in bonito. Thus, it can be said that the structure of this part in bonito ferrous form is rather closer to that of horse ferric form than to that of tuna ferrous form. Although this conformational difference may have something to do with the oxidation and reduction of cytochrome *c* under various conditions, it is also conceivable that this difference may be caused by the packing schemes of the molecules in the two types of crystals. This is, however, not due to the difference in species, because the tetragonal forms of horse and bonito ferric proteins both have the same conformation (*4*).

Regarding the mechanism of electron transfer, which is a main function of this protein, many views have been proposed. Winfield (*10*) suggested the existence of some particular aromatic radicals, through which an electron passes in the molecule. From structure analyses of horse and tuna, Dickerson *et al.* proposed (*5*) that the overlapping of the three aromatic rings plays an essential role as the electron pathway from the reductase through Tyr-74, Trp-59, Tyr-67 to the heme. They stated that this idea is also supported by the effect of chemical modification of Trp-59 by N-bromosuccinamide (*11*, *12*), and that the indole moiety of Trp-59 is a key residue for the reductase activity though not for the oxidase activity. On the other hand, Salemme *et al.* reported, based on an analysis of cytochrome c_2 (*13*, *14*), that reduction of the heme should take place by direct transfer of an electron from an approaching moiety such as a metalloporphyrin, interacting with the cytochrome heme at its front edge, and that this process may be facilitated by the hydrogen bond network.

Considering the quantum mechanics of the charge transfer process between two molecules, Yomosa (*15*) concluded that the charge transfer interaction energy is proportional to $S_{ab'}/R_{ab'}$, where $S_{ab'}=\int \Phi_a \Phi_b d\tau$ is an overlap integral between the donor molecular orbital

(Φ_a) of molecule *a* and the acceptor molecular orbital (Φ_b) of molecule *b* and R_{ab} denotes the effective distance between two orbitals. The molecular orbital is generally represented as a linear combination of the component atomic orbitals, that is, $\Phi_a = \sum_i a_i{}^a \varphi_i{}^a$, and $\Phi_b = \sum_j a_j{}^b \varphi_j{}^b$.

The overlap integral S_{ab} is formulated as

$$S_{ab} = \sum_i \sum_j a_i{}^a a_j{}^b \int \varphi_i{}^a \varphi_j{}^b d\tau = \sum_i \sum_j a_i{}^a a_j{}^b \langle \varphi_i{}^a | \varphi_j{}^b \rangle$$

In order to estimate the interaction between Trp-59 and Tyr-74 in the oxidized form, the molecular orbitals of the indole and phenyl rings were calculated using the Hückel approximation, the parameters of overlap and Coulomb integrals being taken from Hoffman and Ladik (*16*). The value of $\langle \varphi_i{}^a | \varphi_j{}^b \rangle$ is inversely proportional to the distance between related atoms, so that S_{ab} can be roughly estimated from the summation of the overlap integrals between adjacent atoms. From Table VII, the distance $C_6{}^{59} \cdots C_2{}^{74}$, $C_6{}^{59} \cdots C_3{}^{74}$, $C_7{}^{59} \cdots C_2{}^{74}$, and $C_7{}^{59} \cdots C_3{}^{74}$ in the horse ferric form are all nearly equal, and are shorter than the other C···C distances involving Trp-59 and Tyr-74, so that $\langle \varphi_i{}^a | \varphi_j{}^b \rangle$ is estimated to be constant for the above pairs, and to be zero for the other pairs. According to Dickerson, Tyr-74 accepts an electron in the lowest un-

TABLE VII. Interatomic distances within 5.0 A among Trp-59, Tyr-67, and Tyr-74. The nomenclature of each atom is as shown in Fig. 9.

		Bonito	Tuna	Horse
59	67			
C5	C1		4.8A	
C5	C2		4.7	4.2A
C5	C3		4.9	4.0
C6	Cβ		4.0	
C6	C1	4.8A	3.8	4.9
C6	C2	4.8	4.0	3.8
C6	C3	4.9	4.4	4.0
C6	C4	5.0	4.6	
C6	C5	5.0	4.6	
C6	C6	4.9	4.2	
C7	Cβ	4.9	4.2	
C7	C1	4.8	4.5	
C7	C2	4.9	4.8	4.9
59	74			
C6	C3	4.6	4.7	4.7
C6	C3	4.0		5.0
C6	C4	4.9		
C6	OH	5.0		
C7	C2		4.7	4.9
C7	C3		4.3	4.8
C7	OH	4.0	5.0	
C8	C3	4.7		
C8	OH	4.8		
67	74			
Cα	Cβ		4.6A	
Cα	C1	4.7A	4.6	
Cα	C2	3.8	4.2	
Cα	C3	3.8	4.7	
Cα	C4	4.7		
Cβ	C1		4.8	
Cβ	C5		4.2	
C1	C5	4.2	4.6	
C1	C6	4.2	4.1	
C5	C2	4.5	4.3	
C6	Cβ	4.9	4.1	4.9A
C6	C1	4.7	4.1	
C6	C2	3.6	4.1	
C6	C3	4.1	4.2	

TABLE VIII. Calculated coefficients of molecular orbitals using the Hückel approximation.

Trp-59 No.	E	C1	C2	C3	C4	C5	C6	C7	C8	C9
1	2.43	0.31	0.31	0.43	0.48	0.28	0.19	0.18	0.25	0.43
2	1.63	−0.19	−0.38	−0.40	−0.05	0.26	0.46	0.50	0.35	0.07
3	1.26	−0.40	−0.09	0.30	0.29	0.46	0.29	−0.10	−0.41	−0.42
4	0.79	0.12	0.50	0.25	−0.45	−0.16	0.32	0.42	0.01	−0.41
5	0.45	−0.54	−0.18	0.47	0.12	−0.37	−0.29	0.24	0.39	−0.06
6	−0.88	−0.20	0.39	−0.17	−0.14	0.52	−0.31	−0.25	0.53	−0.22
7	−1.24	−0.15	−0.12	0.30	−0.43	−0.04	0.48	−0.56	0.21	0.30
8	−1.15	−0.52	0.55	−0.37	0.24	−0.30	0.22	−0.05	−0.14	0.27
9	−2.16	−0.25	0.05	0.14	−0.45	0.35	−0.31	0.32	−0.38	0.50

Tyr-74 No.	E	C1	C2	C3	C4	C5	C6	OH
1	2.70	0.09	0.13	0.25	0.55	0.25	0.13	0.73
2	1.75	−0.52	−0.45	−0.27	−0.02	−0.27	−0.45	0.42
3	1.00	0.00	−0.50	−0.50	0.00	0.50	0.50	0.00
4	0.68	−0.50	−0.17	0.38	0.43	0.38	−0.17	−0.46
5	−1.00	0.00	−0.50	0.50	0.00	−0.50	0.50	0.00
6	−1.10	−0.57	0.31	0.23	−0.56	0.23	0.31	0.23
7	−2.03	−0.38	0.39	−0.41	0.44	−0.41	0.39	−0.14

occupied orbital (No. 5 in Table VIII) from the reductase. Then, the electron goes towards the lowest antibonding orbital of Trp-59 (No. 6). The S_{ab} of this process is as follows;

$$\begin{aligned} S_{ab} &= (a_6^{59}\cdot a_2^{74} + a_6^{59}\cdot a_3^{74} + a_7^{59}\cdot a_2^{74} \\ &\quad + a_7^{59}\cdot a_3^{74})\cdot\langle\varphi^a|\varphi^b\rangle \\ &= (a_6^{59}+a_7^{59})\cdot(a_2^{74}+a_3^{74})\cdot\langle\varphi^a|\varphi^b\rangle \\ &= (-.031-0.25)\cdot(-0.50+0.50)\cdot\langle\varphi^a|\varphi^b\rangle \\ &= 0.00\cdot\langle\varphi^a|\varphi^b\rangle \end{aligned}$$

This estimate suggests that electron transfer from Tyr-74 to Trp-59 cannot occur, though this calculation is rather rough. In addition, the overlap between Tyr-74 and Trp-59 is not found in horse. Stereoscopic drawings of these rings are shown in Fig. 9, where the parameters of horse and tuna are taken from Dickerson (*17*). Thus, this pathway through the aromatic ring is not plausible under these conditions. It must, however, be emphasized that this conclusion is based on the static structural model with no consideration of dynamical changes of the relative location of the residues.

An extended hydrogen bond network is found in the present model. The hydrogen bonds are between Arg-38···inner P, Asn-52··· outer P, Thr-78···outer P, and probably Asn-52···Thr-78. All the hydrogen bonds, except for Asn-52···outer P, which are found in the ferric form are also observed in the present structure; Tyr-67···Thr-78, and Trp-59··· inner P. These residues are evolutionally conserved, so that this hydrogen bond network is an essential feature of this protein. Thus we may speculate that the hydrogen bonds may play a key role in the process of electron transfer. Figure 3 shows a schematic diagram of the hydrogen bond network in the reduced form. Theoretical treatment (*18*) shows that the charge transfer complex takes an ordinary ground state (F-state, AB) in less polar solvents,

but in polar solvents the polarized conformation (S-state, A^+B^-) is stabilized by the interaction between the dipole of the complex and the reaction field due to the polarization of the medium. Form structure analysis, interaction between Tyr-67 and heme can reasonably be expected, because the rotation of Tyr-67 around the C_β-C_γ bond causes some interaction with the heme plane, or because, as Kraut reported for cytochrome c_2, Tyr-67 interacts with heme through the sulfur atom of Met-80, which is in contact with oxygen atom of the Tyr-67 ring. In the reduced form, this pair is in less polar surroundings, because Phe-82 covers the left channel found in the ferric form. At the first step of oxidation, Phe-82 moves out in the exterior and the complex, heme···Tyr-67 (F-state), is exposed to the polar solvent (water), so that this complex is polarized in the state heme$^+$···Tyr-67$^-$ (S-state). The negative charge on Tyr-67 is transferred to the molecular surface through the hydrogen bond. Arg-38 and Thr-78 are on the molecular surface, linked to this hydrogen bond network. Inner P cannot accept an electron from Tyr-67, because it is negatively charged by transferring of a proton to Arg-38 through the hydrogen bond, so that the electron on Tyr-67 cannot flow to Arg-38 through inner P. This means that Arg-38 is not involved in the transfer of an electron from the present protein. Thr-78 may accept an electron from Tyr-67 on the molecular surface, and the charge on Thr-78 may flow to Tyr-48 which forms a hydrogen bond with Thr-78. The subsequent step is a modulation of the hydrogen bond pattern with removal of the water molecule, because the fixed water molecule is not reported in horse. It has been reported by the authors that ferrocytochrome *c* is oxidized to the ferric form in the crystalline state without drastic conformational changes. In this process, the same pathway as stated above might be plausible, because the interaction between heme and Tyr-67 could be in the S-state to a minimum extent, though the Phe-82 ring covers the left channel. This reaction is unfavorable, judging from the facts that the rate of oxidation in the crystalline state is very slow and the crystal lattice is disrupted when oxidation proceeds beyond 65%.

The trigger of the reduction is the removal of the positive charge on Arg-38 in contact with the reductase. The negative charge on inner P would migrate to Tyr-67 through the hydrogen bond when the positive charge on Arg-38 is neutralized by the reductase. The successive movement of Phe-82 changes the interaction (S-state) of heme and Tyr-67 into F-state. Fixing the water molecule and rearrangement of the hydrogen bond convert the protein into the reduced conformation. Trp-59 is involved in the reduction process because of the hydrogen bond linking it with inner P, but does not contribute to the oxidation process; this idea is supported by the results of chemical modification of Trp-59 (*11*). Another hydrogen bond chain from His-18 to the amido of Glu-44 lies in front of the molecule. This hydrogen bond chain may play a role in other enzymatic reactions, because a recent NMR study of ferrocytochrome *c* (*19*) shows that small anions, inorganic phosphate, ADP, and ATP, bind to ferrocytochrome *c* in the immediate vicinity of His-26. This specula-

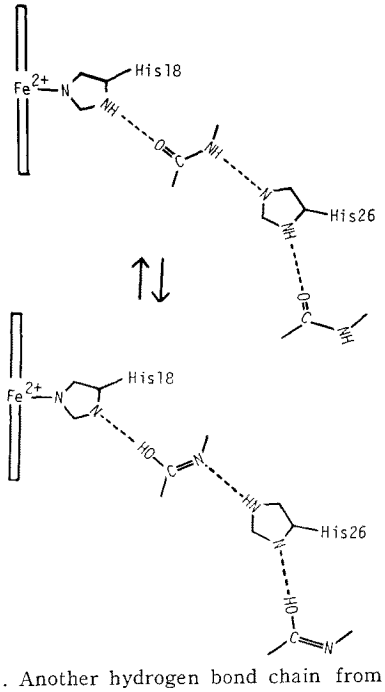

Fig. 11. Another hydrogen bond chain from His-18 to the amido of Glu-44.

tion show that the location of Phe-82, a unique difference between the two states, may be important in the redox process, and that only a slight conformational differences of the molecule is needed for conversion from one state to the other. Kraut *et al.* also reported the importance of hydrogen bonds in the electron transfer mechanism of cytochrome c_2 (*13*, *14*). These speculations concerning electron transfer are plansible on the basis of present physicochemical evidence, but further work is necessary to resolve remaining ambiguities.

The authors wish to express their thanks to the Emeritus Professors Dr. I. Nitta, Dr. S. Akabori, and Dr. K. Okunuki for their encouragement through this study. They are also indebted to Drs. R.E. Dickerson and T. Takano for supplying available data on cytochrome *c*; to Dr. T. Horio for his kind advice; to Drs. K. Narita, K. Titani, and T. Nakayama for their amino acid sequence data; to Dr. S. Yomosa for his suggestion of the quantum mechanical treatment for the electron tranfer process; to Dr. T. Tanaka for his generous gift of $(CH_3)_2SnCl_2$; and to Mr. K. Takeda, the head of the Shizuoka Factory of Daikin Cannery Co., Ltd., for supplying about 500 kg of binito heart. They are also grateful to the Computer Centers of Kyoto University and Osaka University for the use of their computers. The authors are indebted to Miss S. Bando for her valuable help during this study.

This work was partly supported by research grants in 1970 and 1971 from the Ministry of Education of Japan.

REFERENCES

1. Nakayama, T., Titani, K., & Narita, K. (1971) *J. Biochem.* **70**, 311
2. Ashida, T., Ueki, T., Tsukihara, T., Sugihara, A., Takano, T., & Kakudo, M. (1971) *J. Biochem.* **70**, 913
3. Ashida, T., Tanaka, N., Yamane, T., Tsukihara, T., & Kakudo, M. (1973) *J. Biochem.* **73**, 463
4. Tsukihara, T., Yamane, T., Tanaka, N., Ashida, T., & Kakudo, M. (1973) *J. Biochem.* **73**, 1163
5. Dickerson, R.E., Takano, T., Eisenberg, D., Kallai, O.B., Samson, L., Cooper, A., & Margoliash, E. (1971) *J. Biol. Chem.* **246**, 1511
6. Takano, T., Kallai, O.B., Swanson, R., & Dickerson, R.E. (1973) *J. Biol. Chem.* **248**, 5234
7. Blow, D.M. & Crick, F.H.C. (1959) *Acta Cryst.* **12**, 794
8. Cullis, A.F., Muirhead, H., Perutz, M.F., Rossman, M.G., & North, A.C.T. (1961) *Proc. Roy. Soc.* **A265**, 15
9. Venkatachalam, C.M. (1968) *Biopolymers* **6**, 1425
10. Winfield, M.E. (1965) *J. Mol. Biol.* **12**, 600
11. Myer, Y.P. (1973) *Biochemistry* **11**, 4195
12. Ulmer, D.D. (1966) *Biochemistry* **5**, 1886
13. Salemme, F.R., Freer, S.T., Xuong, N.G., Alden, R.A., & Kraut, J. (1973) *J. Biol. Chem.* **248**, 3910
14. Salemme, F.R., Kraut, J., & Kamen, M.D. (1973) *J. Biol. Chem.* **248**, 7701
15. Yomosa, S. (1973) *J. Phys. Soc. Japan* **35**, 1501
16. Hoffman, T.A. & Ladik, J. (1964) *Adv. Chem. Phys.* **7**, 84
17. Brown, J.B., Takano, T., & Dickerson, R.E. private communication
18. Yomosa, S. (1973) *J. Phys. Soc. Japan* **35**, 1738
19. Stellwagen, E. & Shulman, R.G. (1973) *J. Mol. Biol.* **75**, 683